Int. J. Electrochem. Sci., 7 **(2012)** 3750 - 3764

International Journal of
ELECTROCHEMICAL
SCIENCE
www.electrochemsci.org

Study on Hydrogen Evolution Reaction at a Graphite Electrode in the All-Vanadium Redox Flow Battery

Fuyu Chen, Jianguo Liu, Hui Chen, Chuanwei Yan[*]

State Key Laboratory for Corrosion and Protection, Institute of Metal Research, Chinese Academy of Sciences, 62 Wencui Road, Shenyang 110016, China
[*]E-mail: fychen@imr.ac.cn

Received: 15 September 2011 / *Accepted:* 3 December 2011 / *Published:* 1 April 2012

The hydrogen evolution reaction in the negative half-cell of a vanadium redox battery is studied at a graphite electrode. Hydrogen evolution behavior is included by potentiostatic method. It is found that volume of hydrogen evolution goes up linearly at the first stage and then increases slowly at different polarization potential, concentration of sulfuric acid and V^{3+}. The reason is adsorption hydrogen on graphite surface, with a trend toward an increase in electrical resistance and a decrease in the active surface area. The surface morphology and structural properties of graphite are investigated by scanning electron microscope (SEM) and X-ray photoelectron spectroscopy (XPS). The electrochemical performance of graphite is observed using cyclic voltammetry and impedance spectroscopy (EIS). It is shown that hydrogen evolution reaction changes surface morphology and introduces some defect sites on the surface of graphite. The electrochemical activity of graphite towards V^{3+}/V^{2+} couple becomes less easily after hydrogen evolution treatment.

Keywords: hydrogen evolution; graphite; electrochemical activity; vanadium battery

1. INTRODUCTION

Redox flow batteries (RFBs) are electrochemical energy storage devices that utilize the oxidation and reduction of soluble redox couples for charging and discharging. RFBs have several advantages [1-4] over some of the established conventional secondary batteries: long cycle life and relatively easily maintained; high battery efficiency; environmental friendly; deeply discharged without harm to the battery. So the RFB is thought to be ranked as the most promising one for the application of large scale energy storage among the electrochemical storage systems [5-6]. They are appropriate for load leveling, uninterruptible power supply and distributed renewable power plants such as solar power plants and wind power plants.

Since the RFB concept was first proposed by Thaller [7] in 1974, several types of redox flow batteries have been developed [8-9]. For example, all-vanadium redox flow battery (VRB) system, which received considerable attention during the last years [10-13], employed two redox couples of VO_2^+/VO^{2+} and V^{3+}/V^{2+} as the positive and the negative electrode active materials, respectively. The positive and the negative electrolyte which containing VO_2^+/VO^{2+} and V^{3+}/V^{2+} active materials are stored in each electrolyte tanks and flowed through the electrode compartment by pumps. The capacity of the system is determined by the volume of the electrolyte tanks, while the system power is determined by the size of the stacks and the active electrode surface area. In contrast to usual secondary batteries which using solid active materials, VRB has a long cycle life and relatively large capacitance.

Despite these advantages, the vanadium redox flow battery has not been widely exploited to date. One disadvantage of the system developed to date is the imbalance in capacity losses of the positive and negative half-cell caused by oxygen and hydrogen evolution in electrode compartments. Gas evolving reactions are consuming a portion of the current applied to the cell, reducing active surface area for reaction [3], which speeds up charge and discharge imbalances and finally leads to declining of coulombic efficiency, energy efficiency and the capacity after repetitious systemic circulation of the battery. Therefore, it is important to understand the factors affecting the performance of gas evolution reaction for acceptable performance and longevity of the cell.

In this paper, behavior of hydrogen evolution at a graphite electrode was studied at the first section. Secondly, general surveys for the surfaces microstructure characterizations, structural properties and electrochemical performance of before and after hydrogen evolution treatment samples were reviewed. These experiments aimed to provide a preliminary indication of the relative performance of hydrogen evolution reaction.

2. EXPERIMENTAL

2.1. Electrolytes

Electrolytic solutions were prepared by fully discharging of VO^{2+} solution to V^{3+} in the negative half-cell of a vanadium redox cell. The electrolytic for cyclic voltammetry and electrochemical impedance spectroscopy were 0.1M V^{3+} + 1M H_2SO_4. All chemicals were analytical reagent grade.

2.2. Hydrogen evolution measurements

The graphite electrodes with a surface area of 1.33 cm^2 (spectroscopically pure) were polished with 2000 CCR/R silicon carbide polishing paper and polishing cloth, followed successively by 10 min ultrasonic cleaning and then rinsed thoroughly with distilled water. The onset of hydrogen evolution on graphite fiber electrode occurs at −0.7 V (vs. SCE) in 1 M sulfuric acid [14]. Therefore, the hydrogen collection experiments were studied at different negative polarization potentials (started from −0.7 V),

concentration of sulfuric acid and V^{3+} electrolytic. Hydrogen evolution was gathered by the drainage method. Three-electrode electrochemical cell and gas collection device were shown in Fig. 1.

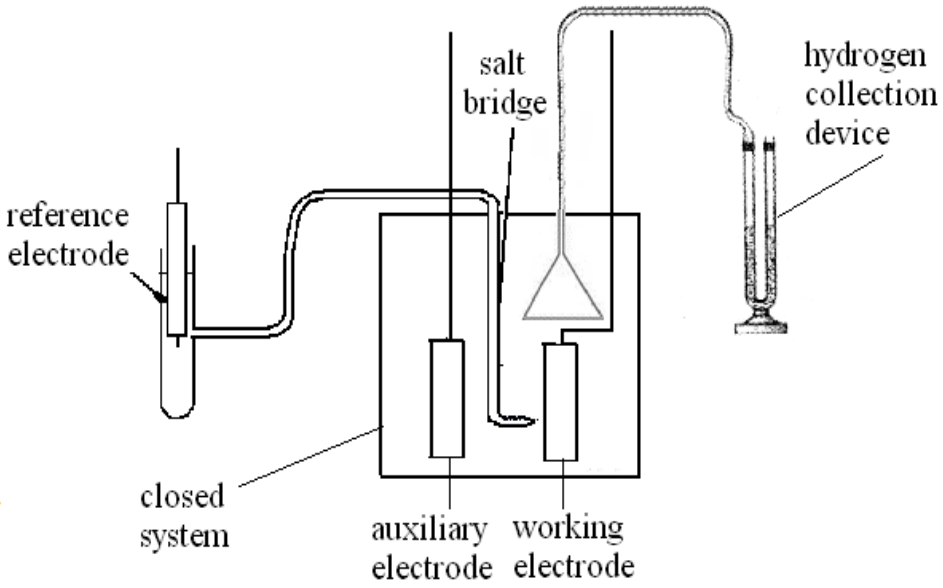

Figure 1. Electrolytic cell and gas collection device

Electric quantity consumed by reaction of $V^{3+} \rightarrow V^{2+}$ was achieved by definite integral of current-time curve subtracted electric quantity consumed by hydrogen evolution under given potential. The coulombic efficiency of $V^{3+} \rightarrow V^{2+}$ reaction was obtained by electric quantity consumed by the reaction divided electric quantity of definite integral of current-time curve under given potential as shown in Eq. (1, 2, 3).

$$Q = I \times t = \int_0^t Idt \qquad (1)$$

$$Q_{H2} = \frac{V_{H2}}{22.4} \times nF \qquad (2)$$

$$\eta_{V3+ \rightarrow V2+} = \frac{Q - Q_{H2}}{Q} \times 100\% \qquad (3)$$

2.3. Characterization of graphite electrode

The surface morphology of the graphites was examined using a XL30FEG scanning electron microscope (SEM) (FEI Company Inspect F, Japan). X-ray photoelectron spectroscopy (XPS) measurements were performed in an ultra-high vacuum set-up equipped with Al K_α X-ray source

generated at 15 kV and 10mA employing ESCA-LAB250 surface analysis system. The base pressure in the measurement chamber was about 6.0×10^{-8} mbar.

2.4. Electrochemical measurements

The electrochemical measurements were performed using a Princeton Applied Research (PAR) EG&G potentiostat model 273 and EG&G5210 lock-in amplifier with M398 testing software. All electrochemical measurements were conducted using a conventional three-electrode electrochemical cell with graphite as working electrode, a platinum plate as auxiliary electrode and a saturated calomel (SCE) as reference electrode. The scan rate of cyclic voltammetry was 50 $mV\cdot s^{-1}$. The signal amplitude of EIS was 5 mV and the frequency ranged between 1.0E-2 Hz and 1.0E-5 Hz. All the electrochemical measurements were conducted at room temperature.

3. RESULTS AND DISCUSSION

3.1. Hydrogen evolution behavior

The variation in hydrogen evolution volume with time and the coulombic efficiency of $V^{3+}\rightarrow V^{2+}$ reaction on graphite electrodes at different negative polarization potentials are shown in Fig. 2. The hydrogen evolution rate becomes more significant with increasing of polarization potential (Fig. 2(a)). At a given polarization potential, the rate of hydrogen evolution goes up linearly at the first stage and then changes slowly as time up to 10h at each polarization potential. The reason may be caused by adsorption hydrogen on graphite surface which reduces active area and increases the electrical resistance of electrode [15-16]. The adsorption hydrogen atoms combine with each other and form gas of hydrogen. Characteristic of gas evolving cells is the formation of gas bubbles. The presence of the bubbles reduces active surface area of electrode [3], thus restrains reaction of hydrogen evolution. The behavior of hydrogen evolution at potential of −1.0 V is quite different, the reason may be caused by adsorption atomic hydrogen reacts with carbon and forms hydrocarbon leaving the surface of graphite which decreases adsorption hydrogen on the surface of graphite [17]. The coulombic efficiency reduces gradually corresponding to different negative potentials is presented in Fig. 2(b), which suggests that the decrease of coulombic efficiency is consistent with hydrogen evolution volume.

Hydrogen evolution behavior and coulombic efficiency at polarization potential of −0.9 V in different concentration of sulfuric acid (0.1M V^{3+}) is shown in Fig. 3. The performance is similar with that of different negative potential. The volume of hydrogen evolution has the maximal values in 1M sulfuric acid and the condition corresponds to the minimal coulombic efficiency for $V^{3+}\rightarrow V^{2+}$ reaction. As the concentration of sulfuric acid increased (less than 1M), the contents of H^+ on the surface of electrode is increased, the reaction rate of H^+ speeds up accordingly. Therefore, the volume of hydrogen evolution increases. At the same time, the viscosity of electrolyte goes up with increasing concentration of sulfuric acid. When the concentration of sulfuric acid exceeds 1M, the diffusion rate of H^+ reduces which results in slow rate of hydrogen evolution. The variation of hydrogen evolution

volume is consistent with coulombic efficiency for $V^{3+} \rightarrow V^{2+}$ reaction. Fig.4 shows hydrogen evolution behavior and coulombic efficiency at potential of −0.9V in different concentration of V^{3+} (1M H_2SO_4). The hydrogen evolution volume decreases gradually and the coulombic efficiency of $V^{3+} \rightarrow V^{2+}$ reaction increases as the concentration of V^{3+} added. The reason is that increasing of concentration of V^{3+} accelerates the reaction rate of $V^{3+} \rightarrow V^{2+}$ while restrains the reaction of hydrogen evolution at the fixed graphite electrode.

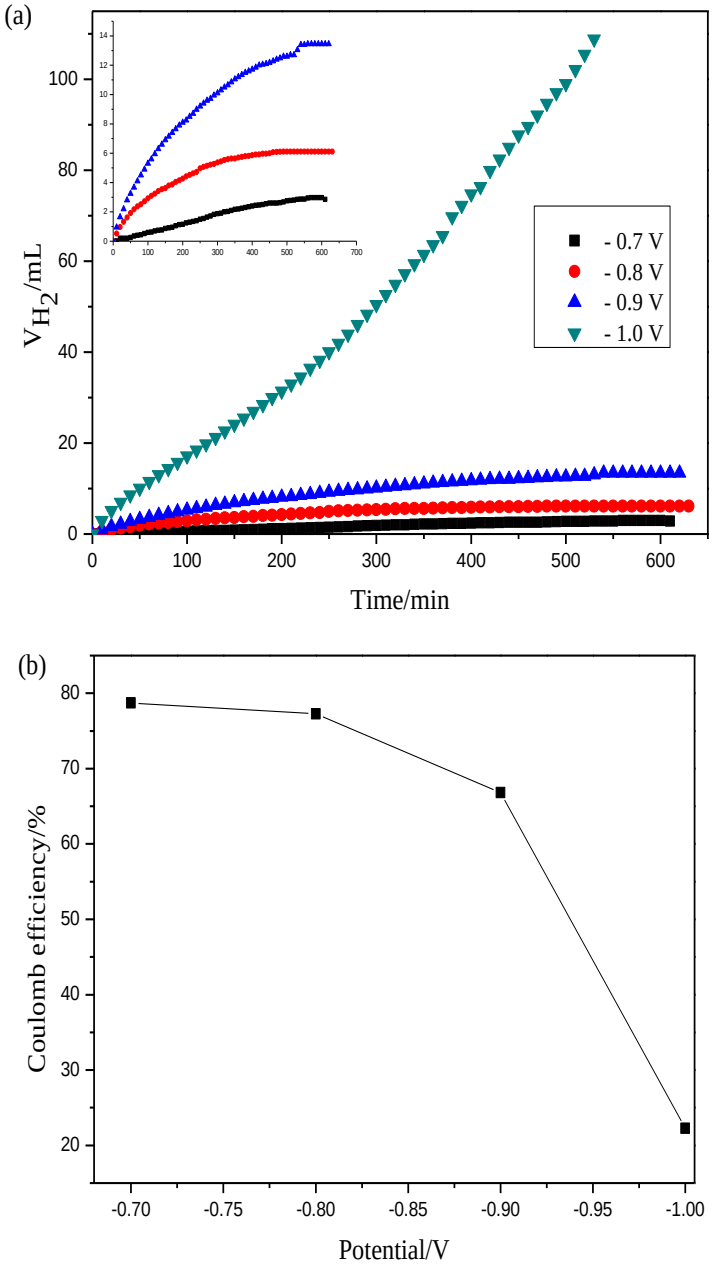

Figure 2. Hydrogen evolution behavior(a) and coulombic efficiency(b) at different negative potentials in 0.1M V^{3+}+2M H_2SO_4

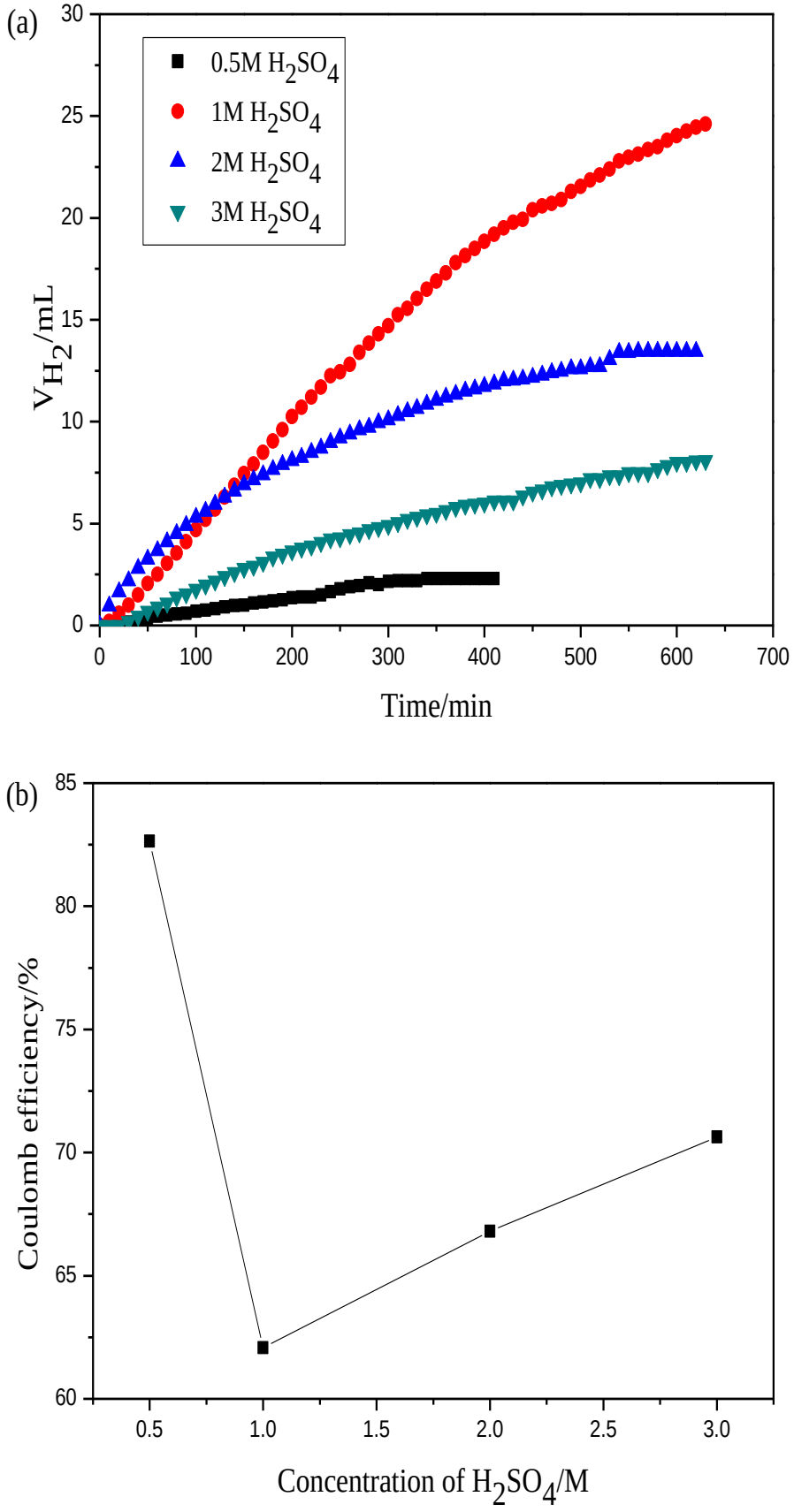

Figure 3. Hydrogen evolution behavior(a) and coulombic efficiency(b) at potential of −0.9 V in different concentration of sulfuric acid(0.1M V^{3+})

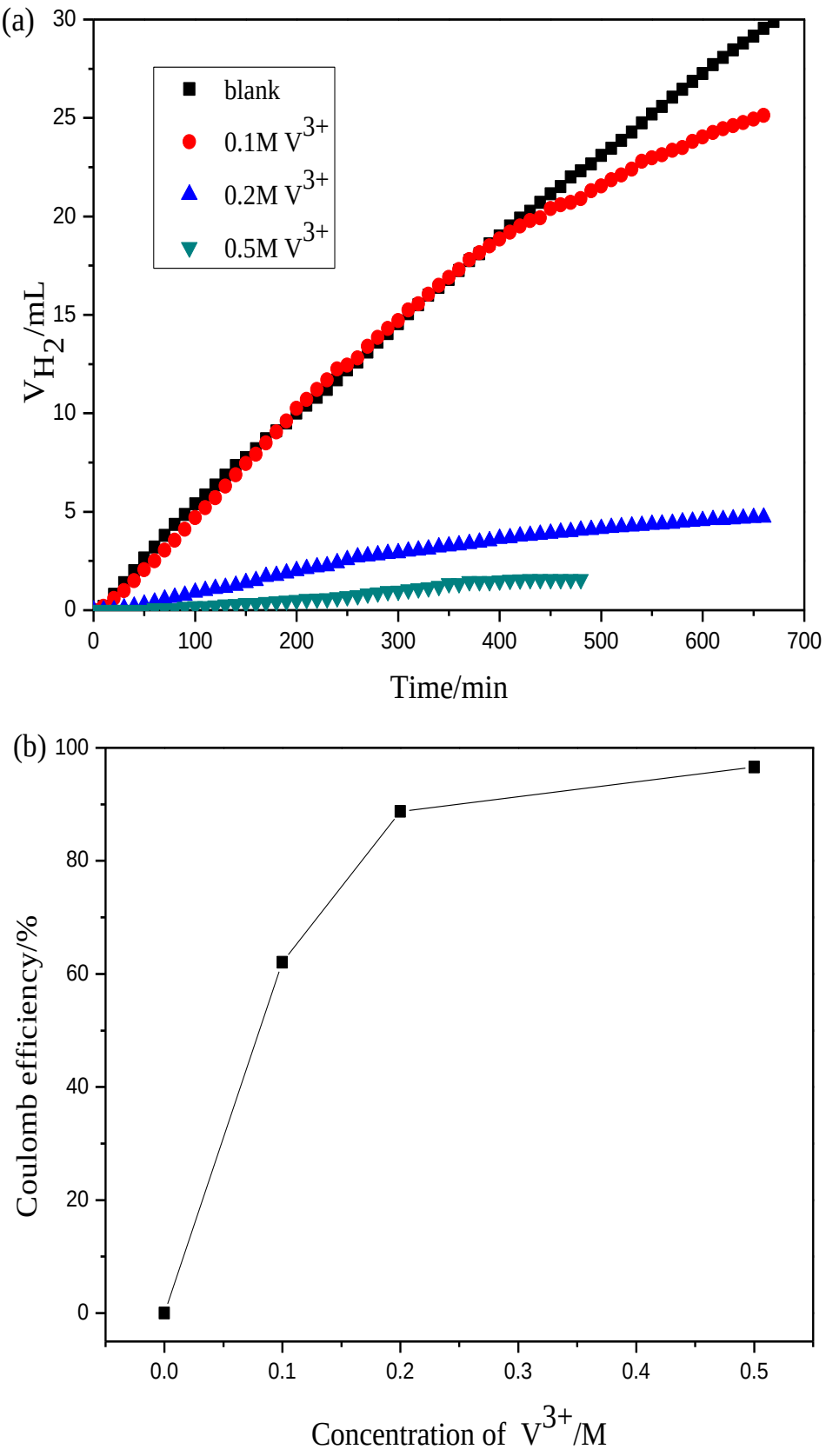

Figure 4. Hydrogen evolution behavior(a) and coulombic efficiency(b) at potential of −0.9 V in different concentration of V^{3+} (1M H_2SO_4)

3.2. Microstructure characterizations and structural properties

The surface morphology of the graphites electrode both before and after potentiostatic cathodic polarization is illustrated in the Fig. 5.

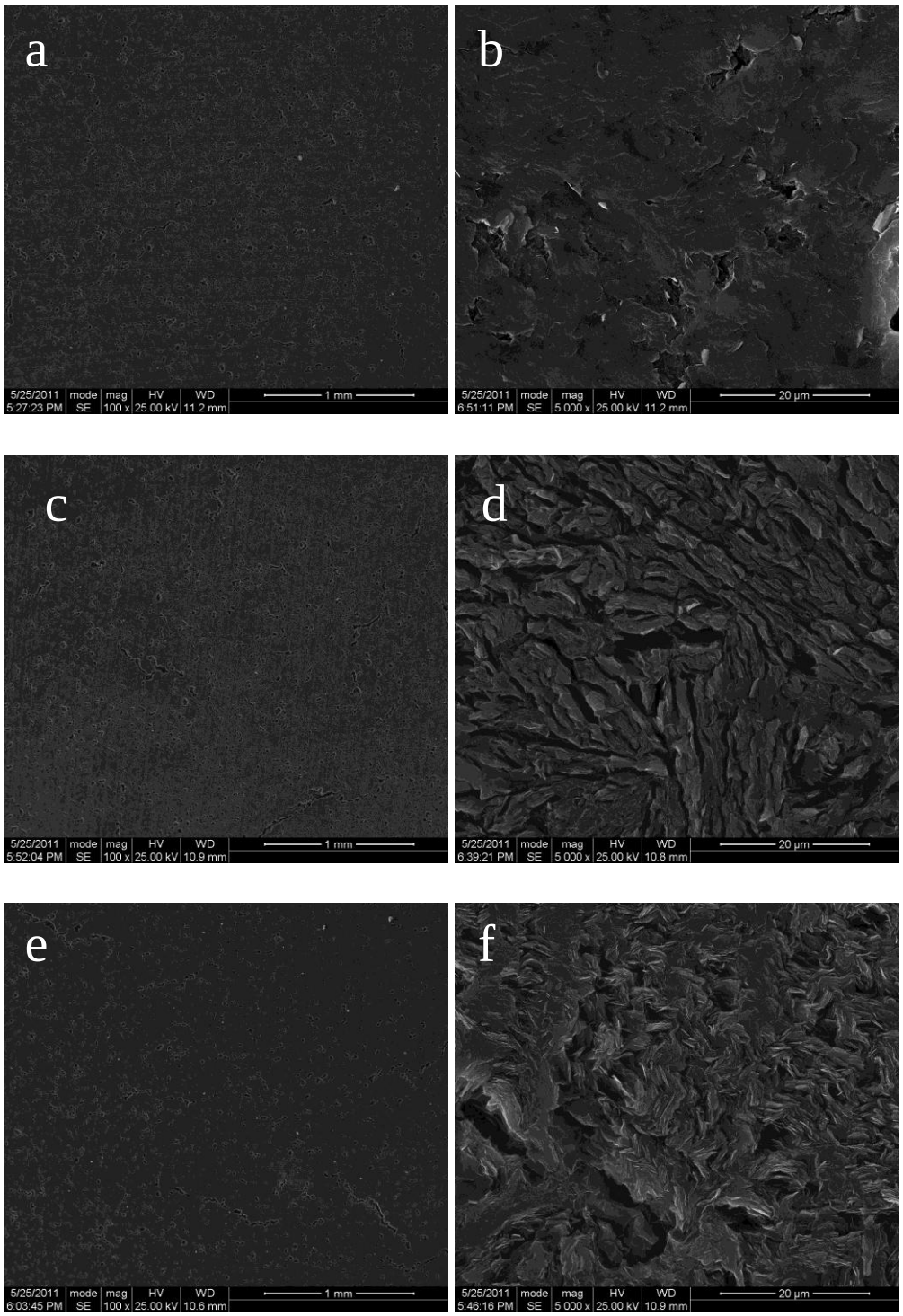

Figure 5. Scanning electron micrograph for graphites electrode before and after potentiostatic cathodic polarization: (a), (b) pristine; (c), (d)−0.9 V-10h; (e); (f)−1.0 V-10h.

It is clear that there is little difference in the surface condition of the pristine and treatment samples shown in Fig. 5(a), (c), (e). The result reveals that hydrogen evolution does not lead to corrosion of graphite obviously.

From the high magnification images shown in Fig. 5(b), (d), (f), the physical state of the surface for the graphite after hydrogen evolution treatment becomes rough, and the rough degree increases with the increase of the negative potential on the electrodes. This indicates that hydrogen evolution changes the surface microstructure of graphite and introduces some defect sites on the graphite surface by the potentiostatic cathodic polarization.

The results from XPS measurements are shown in Fig. 6. Wide scan spectra in the binding energy range 0~ 800 eV are obtained to identify the surface elements. It can be noted that the amount of oxygen on the treatment graphite surface has decreased.

Curve fittings of the C1s and the O1s for both samples are shown in Fig. 7. The C1s core level peak position of the graphite is approximately at 284.4eV [18]. A slight change in binding energy <0.3eV is considered insignificant based on the energy resolution of XPS instrument used. The C1s spectra of the samples can be fitted by convoluting three peaks, each representing a separate carbon bond, namely, C=C, C–C, C–H (284.4eV), C–OH, C–O–C(286.1~ 286.3eV) and π–π* (290.5 eV)[18] (Fig. 7). The percentage of graphitic/hydrocarbon (C=C, C–C, C–H) groups increases on the surface of graphite after potentiostatic cathodic polarization for 10 h, while the content of C–OH, C–O–C groups reduces. This phenomenon can be explained as part of C–OH, C–O–C bonds on the surface of graphite are broken and combined with adsorption hydrogen atoms to form water molecules which make the groups decrease and the corrosion of graphite surface [19]. On the other hand, C–C group chemisorbes hydrogen atoms [16] and tends to increase C–H group on the graphite surface.

The curve fitting routine of oxygen is shown in Fig. 7. The peak position for oxygen is centred at around 532.0eV confirming the presence of some hydroxyl functional groups on the graphite. The O1s spectra reveals the presence of peak corresponding to oxygen atoms in hydroxyls (–OH) or ethers (C–O–C) (532.2~ 533eV) [20].

A significant 24.25% drop in the peak area of C–OH, C–O–C groups on the graphite surface when the sample is potentiostatic cathodic polarization for 10 h (Fig. 7). The reduced area of C–OH, C–O–C groups corresponds to decreases active sites used for catalyzing the V^{3+}/V^{2+} processes. As described in a separate paper [21], the mechanism of catalysis for the V^{3+}/V^{2+} reaction on the electrode surface can be hypothesized as follows (charge process).

$$C–O–H + V^{3+} \xrightarrow{\text{ion-exchange}} C–O–V^{2+} + H^{+} \quad (4)$$

$$C–O–V^{2+} \xrightarrow{\text{electron transfer}} C–O–V^{+} \quad (5)$$

$$C–O–V^{+} + H^{+} \xrightarrow{\text{ion-exchange}} C–O–H + V^{2+} \quad (6)$$

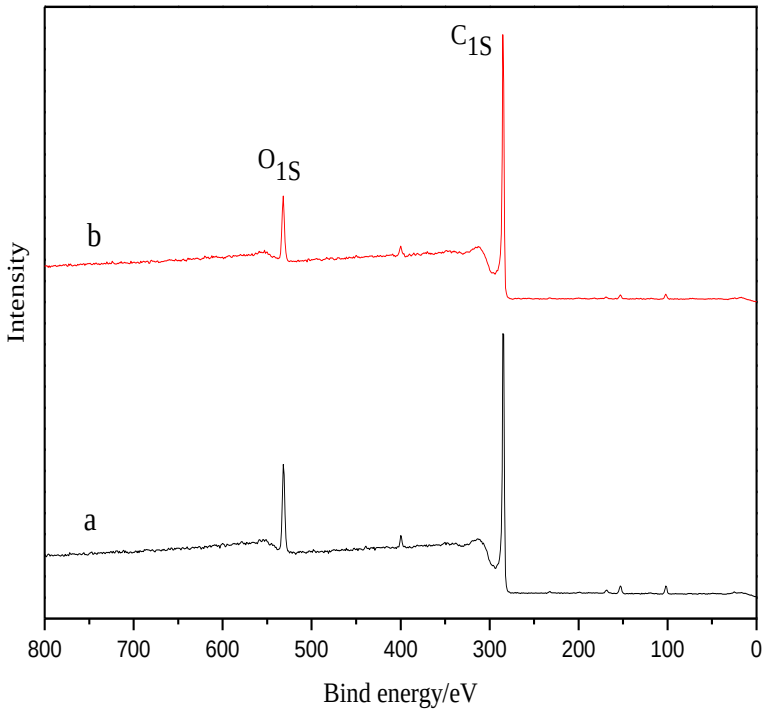

Figure 6. XPS survey spectra of graphite electrode before and after potentiostatic cathodic polarization: (a) pristine; (b) –1.0V-10h

For the discharge process, the reaction is the reverse process of charge. The fact (Eq. (4, 5, 6)) suggests that C–OH and C–O–C functional groups facilitates the process of V^{3+}/V^{2+} redox couple, so that hydrogen evolution treatment restrains activity of graphite and increases the cell resistance in the negative half-cell.

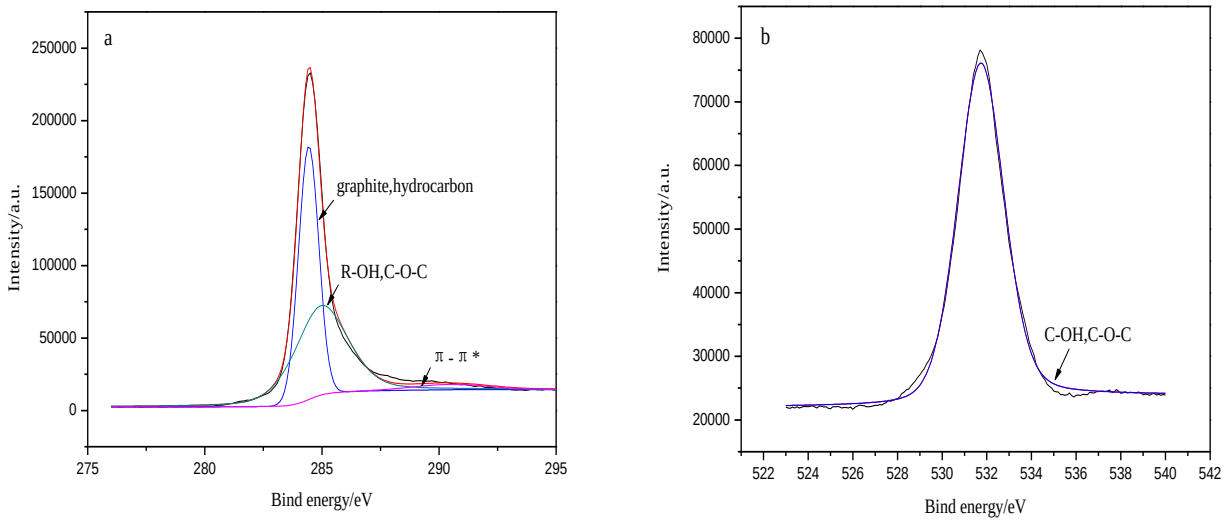

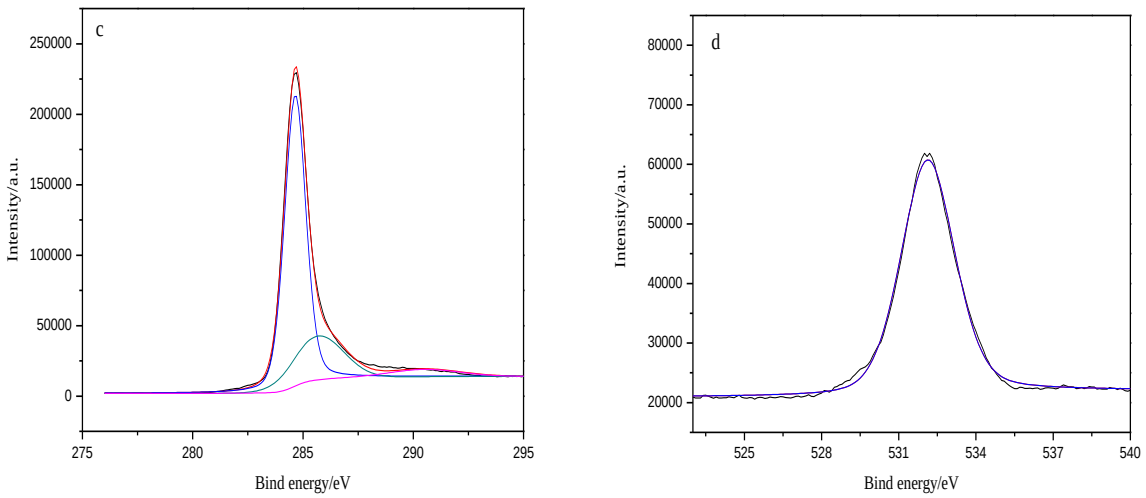

Figure 7. XPS general spectra and curve-fit of C1s and O1s spectra from the as-received graphite before and after potentiostatic cathodic polarization: (a), (b) pristine; (c), (d) –1.0V-10h.

3.3. Electrochemical measurements

A series of cyclic voltammograms corresponding to different polarization potential treatment graphite electrodes for 10h in 0.1M V^{3+} + 1M H_2SO_4 solution at −0.7V, −0.8V, −0.9V and −1.0V is presented in Fig. 8.

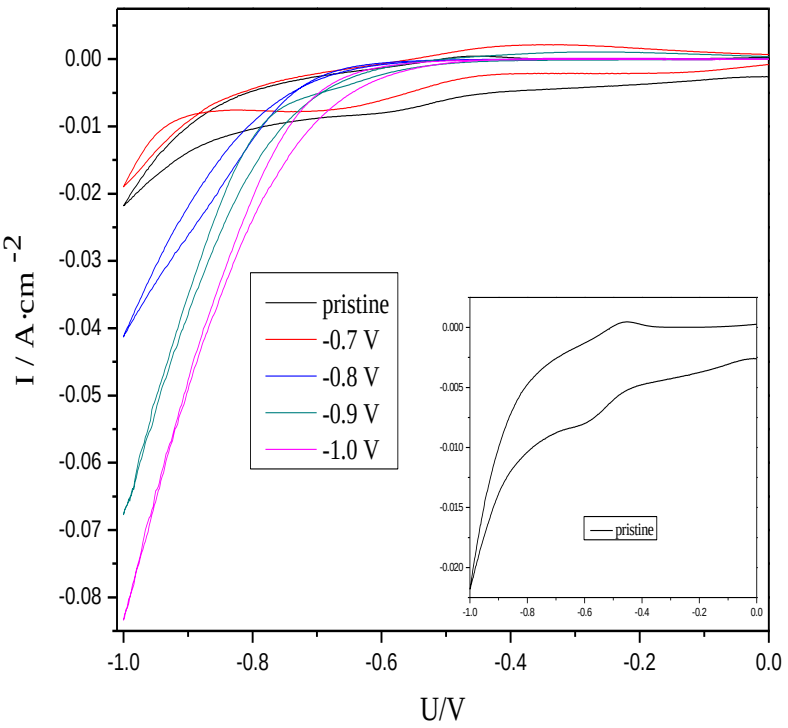

Figure 8. Cyclic voltammograms for graphite electrodes before and after potentiostatic cathodic polarization, sweep rate: 50 $mV \cdot s^{-1}$

The oxidation and reduction peak of V^{3+}/V^{2+} couple can be detected at pristine graphite electrode between the sweeping voltage ranges of −1.0~ 0V. As the separation of two peaks is more than 60mV, the reaction of V^{3+}/V^{2+} couple is irreversible at the pristine graphite electrode. After the graphites are treated with 10h of cathodic polarization treatment, the electrochemical activity towards V^{3+}/V^{2+} couple becomes less easily while the reaction of hydrogen evolution takes place more favorable gradually. It can be ascribed to the decrease of ethers (C−O−C) and hydroxyl (−OH) functional groups on the graphite surface. The two functional groups behave as active sites that are supposed to catalyze the V^{3+}/V^{2+} processes [21-22]. This is in agreement with the result from the XPS. Therefore, hydrogen evolution not only consumes a portion of the current applied to the cell but also restrains reaction activity of V^{3+}/V^{2+} couple.

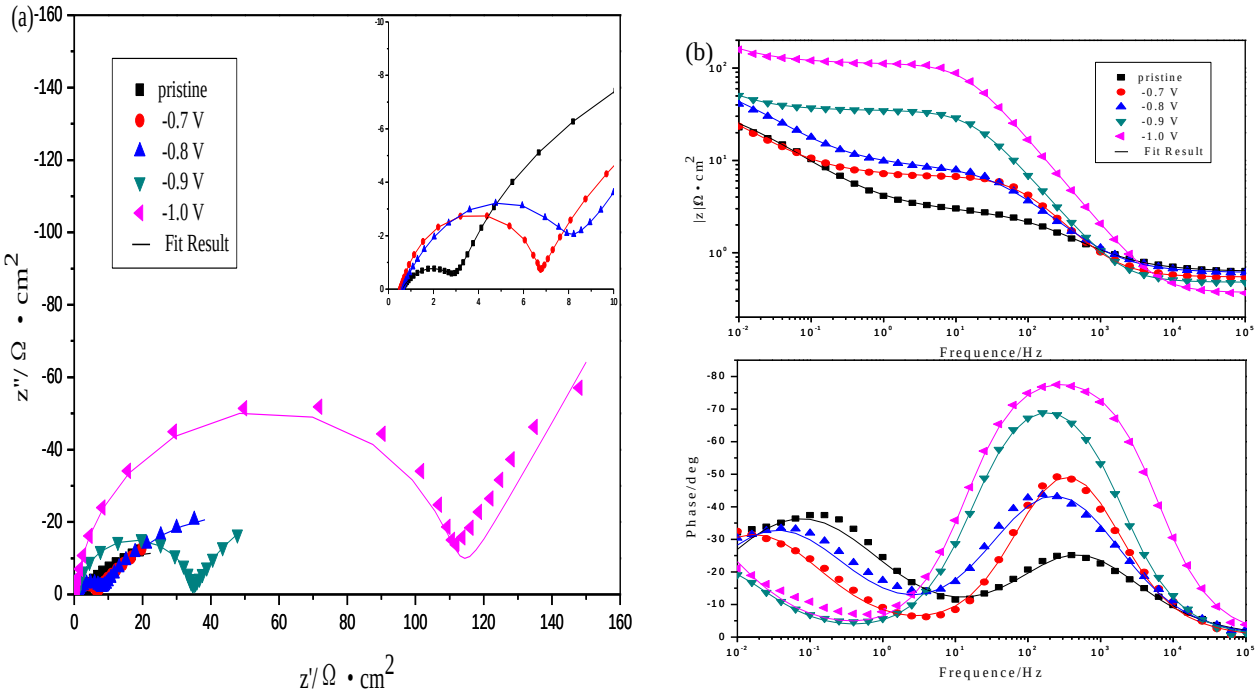

Figure 9. EIS plots for graphite electrodes before and after potentiostatic cathodic polarization at polarization potential of −0.5 V vs. SCE: (a)Nyquist plots; (b)Bode plots

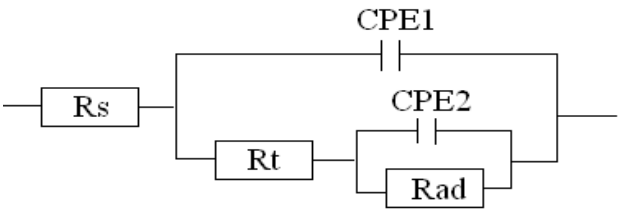

Figure 10. Equivalent circuits proposed for fitting of EIS plots in Fig. 9, Rs is the electrolyte resistance, Rt is the charge transfer resistance, corresponding to resistance of electrode reaction, CPE1 is the constant-phase element used to replace Cp, the double layer capacitance, Rad is the adsorption resistance, corresponding to resistance of adsorption hydrogen, CPE2 is the constant-phase element used to replace Cad, the adsorption capacitance.

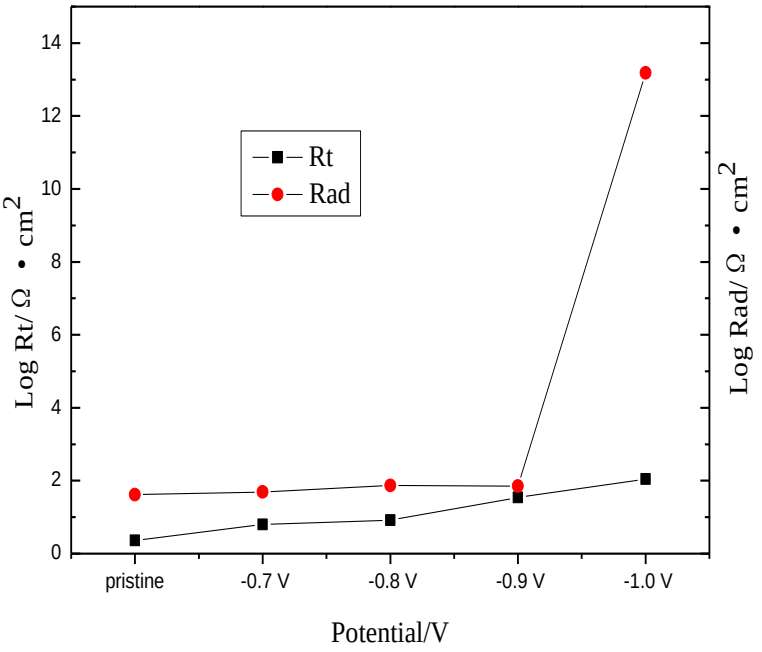

Figure 11. Fitting parameters of Rt and Rad before and after potentiostatic cathodic polarization

EIS diagrams for graphite electrodes before and after treatment at polarization potential of −0.5V are presented in Fig. 9. In 0.1M V^{3+} + 1M H_2SO_4 solution, the impedance spectra exhibits two capacitive features. According to cyclic voltammograms in Fig. 8, both V^{3+}/V^{2+} and H^+/H_2 couples react on the electrode at the potential of −0.5V. The reaction of V^{3+}/V^{2+} couple is the major reaction on the pristine graphite electrode, while H^+/H_2 reaction becomes more important on treatment graphite electrodes. So, the high frequency capacitive feature could be attributed to the charge transfer for V^{3+}/V^{2+} and H^+/H_2 couples, and the low frequency corresponds to adsorption of intermediates [23]. Plots in Fig. 9 can be described using the equivalent circuit shown in Fig. 10.

As shown in Fig. 9(a), it is remarkable that the diameters of semicircles in high frequency increase with the polarization potential from pristine to −1.0V, which suggests the increase in the charge transfer resistance (Fig. 11) caused by adsorption of hydrogen atoms. The result validates that electrical resistance of graphites are increased after the potentiostatic cathodic polarization and the values are proportional to the adsorption hydrogen content. The phase angles in high frequency in the Bode plots (Fig. 9(b)) are related to the electrical double layer, and gradually increase from approximately −25º to −77º from pristine to −1.0V treatment. The value from −25º to −45º corresponds to a porous and highly inhomogeneous surface. For the −1.0V treatment electrode a phase angle of −77º can be calculated, this value may be indicating that adsorption of hydrogen atoms on the electrode surface which blocks the electroactive pores and cavities, so that the electrode behaves like a flat homogeneous surface [24] which indicates a decrease in the reaction rate on the electrode surface.

The capacitive loops in the low frequency correspond to adsorption of hydrogen atoms [23]. The diameters of semicircles increase with the treatment potential from pristine to −1.0V, which suggests the decrease of the adsorption atoms of hydrogen on the electrode surface. The reason is that

active surface area tends to reduce after potentiostatic cathodic polarization. The Bode plots (Fig. 9(b)) in the low frequency presents adsorption capacitive semicircles. The phase angles move to low frequency from pristine to −1.0V treatment, which indicates that resistance of adsorption intermediates increase gradually (Fig. 11). This could be validated by the value of |Z| in the low frequency, which increases from 22 to 158Ω•cm^2 from pristine to −1.0V negative potentials treatment electrodes.

4. CONCLUSIONS

The volume of hydrogen evolution on graphite electrode is notably dependent on the polarization potential, concentration of sulfuric acid and the concentration of V^{3+}. At a given concentration of sulfuric acid and V^{3+}, the volume of hydrogen evolution increases with higher cathodic polarization potential and at a given polarization potential and concentration of sulfuric acid, the volume of hydrogen evolution decreases with the concentration of V^{3+} increased. At a given polarization potential and the concentration of V^{3+}, the volume of hydrogen evolution has the maximal values in 1M sulfuric acid. The variation of coulombic efficiency is consistent with the volume of hydrogen evolution.

Hydrogen evolution reaction occurs on the graphite electrode can lead to adsorption of hydrogen atoms on the surface of graphite which increases the electrical resistance of graphite and the values are proportional to the adsorption hydrogen content. The functional groups of C–OH and C–O–C on the surface of graphite combine with adsorption hydrogen atoms and then form water molecules which make the decrease of the amount of C–OH and C–O–C and the corrosion of graphite surface. The decrease of the amount of functional groups restrains the electrochemical activity towards V^{3+}/V^{2+} couple.

ACKNOWLEDGEMENT
Funding for this research was provided by the Key Basic Research Program (973) of China (2010CB227203).

References

1. H. Al-Fetlawi, A. A. Shah and F. C. Walsh, *Electrochim. Acta* 55 (2009) 78
2. H. Al-Fetlawi, A. A. Shah and F. C. Walsh, *Electrochim. Acta* 55 (2010) 3192
3. A.A. Shah, H. Al-Fetlawi and F. C. Walsh, *Electrochim. Acta* 55 (2010) 1125
4. A.Hazza, D. Pletcher and R. Wills, *J. Powe Sources* 149 (2005) 103
5. C. Ponce de León, A. Frías-Ferrer, J. González-García, D. A. Szánto and F. C. Walsh, J. *Power Sources* 160 (2006) 716
6. Ch. Fabjan, J. Garche, B. Harrer, L. Jo¨rissen, C. Kolbeck, F. Philippi, G. Tomazic and F. Wagner, *Electrochim. Acta* 47 (2001) 825
7. L. H. Thaller, US Patent 3,996,064, US, 1976
8. Y. H. Wen, J. Cheng, H. M. Zhang and Y. S. Yang, *Batttery Bimonthly* 38 (2008) 247
9. M. H. Chakrabarti, R. A. W. Dryfe and E. P. L. Roberts, *Electrochim. Acta* 52 (2007) 2189
10. M. Rychcik and M. Skyllas-Kazacos, *J. Power Sources* 22 (1988) 59

11. E. Sum, M. Rychcik and M. Skyllas-Kazacos, *J. Power Sources* 16 (1985) 85
12. S. Zhong and M. Skyllas-Kazacos, *J. Power Sources* 39 (1992) 1
13. G. Oriji, Y. Katayama and T. Miura, *Electrochim. Acta* 49 (2004) 3091
14. L. Nacamulli and E. Gileadi, *J. Appl. Electrochem*. 12 (1982) 73
15. M. L. Studebaker, *Rubber Chem. Technol*. 30 (1957) 1401
16. D. M. Chen, T. Ichikawa, H. Fujii, N. Ogita, M. Udagawa, Y. Kitano and E. Tanabe, *J. Alloys Compd.* 354 (2003) L5
17. B. Mccarroll and D. W. Mckee, *Carbon* 9 (1971) 301
18. R. I. R. Blyth, H. Buqa, F. P. Netzer, M. G. Ramsey, J. O. Besenhard, P. Golob and M. Winter, *Appl. Surf. Sci*. 167 (2000) 99
19. A.Jelea, F. Marinelli, Y. Ferro, A. Allouche and C. Brosset, *Carbon* 42 (2004) 3189
20. K. Laszlo, E. Tombacz and K. Josepovits, *Carbon* 39 (2001) 1217
21. B. Sun, M and Skyllas-Kazacos, *Electrochim. Acta* 37 (1992) 2459
22. L. Yue, W. Li, F. Sun, L. Zhao and L. Xing, *Carbon* 48 (2010) 3079
23. X. Jiang, *Acta physico-chimica sinica* 9 (1993) 129
24. E. B. Castro, M. J. de Giz, E. R. Gonzalez and J. R. Vilche, *Electrochim. Acta* 42 (1997) 951